ELECTRONIC SUPPLEMENTAL INFORMATION (ESI): Lab on a Chip

Waveguide micro-opto-electro-mechanical resonant chemical sensors

Marcel W. Pruessner, Todd H. Stievater, Mike S. Ferraro, William S. Rabinovich,
Jennifer L. Stepnowski and R. Andrew McGill

S.1 Optical Quality Factor

Typical optical Q-factors for the Fabry-Perot resonances were $Q_{Optical}$=1,600 (*FWHM*=1.0 nm, *FSR*=3.53 nm, finesse *F*=3.5 at λ_0=1604.7 nm). The optical performance is modest due to the long cavity length, L_C, which introduces additional cavity loss. We also intentionally designed some of the air gaps of the DBR mirror to be larger than $\lambda/4$ to reduce squeeze-film damping. Both design changes introduce optical loss and reduce $Q_{Optical}$. Previous fixed Fabry-Perot filters (no MEMS resonators), which have been optimized for their optical performance, have exhibited $Q_{Optical}$>100,000 [S-1] and finesse *F*=496 [S-2]. The present devices are used as MEMS resonant sensors, so high $Q_{Optical}$ and finesse are not a strict design requirement. Furthermore, we use electrostatic actuation [S-3] to actively drive the beam resonances. Consequently, we can counter the reduced displacement sensitivity (and lower finesse) in the present devices by simply increasing the driving voltage.

S.2 Mechanical Quality Factor

Previous MEMS Fabry-Perot filters exhibited $Q_{Mechanical}$=5.2 (f_0=279.2 kHz), $Q_{Mechanical}$=12.2 (f_0=833.6 kHz), and $Q_{Mechanical}$=22.1 (f_0=1.592 MHz) [S-3]. These devices had an air gap of 1 μm separating the MEMS beam and the actuation electrodes. Squeeze-film damping is significant for small air gaps and has a dependence L_{Beam}/gap^3 [S-4]. We therefore increased the air gap to 2 μm in the present devices, which should decrease squeeze-film damping significantly. Figure S2-1 shows two mechanical resonance modes for our sensor. The first is the fundamental mode that we use for sensing and has $Q_{Mechanical}$=11.5 (f_0=149.47 kHz); the next higher-order mode has $Q_{Mechanical}$=40.4 (f_0=576.75 kHz). We achieve an increase in $Q_{Mechanical}$ by a factor of two compared to previous devices [S-3]. The increase is modest, indicating that $Q_{Mechanical}$ is limited by other factors, including anchor/support loss, in addition to squeeze-film damping. A larger increase in *gap* and decrease in L_{Beam} should help to further increase $Q_{Mechanical}$. Ultimately, the mechanical Q-factor determines the minimum resolvable resonant frequency shift and hence the minimum detectable mass-loading. A decrease in air pressure will undoubtedly increase $Q_{Mechanical}$ – indeed, $Q_{Mechanical}$>100,000 has been achieved for silicon resonators tested in vacuum (1 mTorr) [S-5] – however, chemical sensors need to be operated at atmospheric pressures in order to be practical.

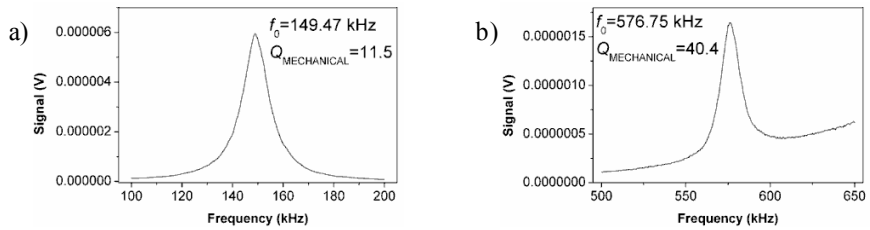

Fig. S2-1: Measured mechanical resonances for an uncoated MEMS resonator with 2 μm air gap. The addition of the PEI coating on the paddles does not negatively impact the mechanical Q-factor.

S.3 Packaging and Optical Loss

The Fabry-Perot optical resonances were measured before and after packaging. The Plexiglas flow cell is attached to the MEMS chip using an optical epoxy (Epoxy Technology, Epotek 310). After curing at 60 °C, the flow cell is attached to the circuit board and MEMS chip with screws. The epoxy forms an "O-ring" seal on top of the input and output optical waveguides, thereby effectively sealing the sensor. We measured the Fabry-Perot optical spectrum before and after packaging and observed no shift in the resonances with negligible optical loss (<0.5 dB, Fig. S3-1).

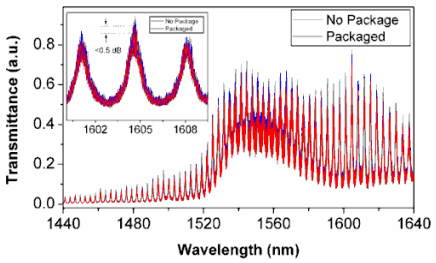

Fig. S3-1: Measured Fabry-Perot resonances before and after flow-cell packaging using an optical epoxy. The additional optical loss is <0.5 dB with no change in the optical resonant spectrum.

S.4 Estimate of Absolute Beam Displacement

The absolute MEMS beam displacement for a given RF actuation is extracted as follows. First, the Fabry-Perot optical resonances are measured. We then find the wavelength that gives the maximum slope (in V/nm). Here, the "nm" unit refers to wavelength and not displacement, while "V" is the measured detector output voltage. Next, we fix the wavelength (λ=1604.690 nm, slope=0.714 V/nm at P=1 mW laser input power) as in Fig. S4-1a and drive the bridge using the RF output from the Network analyzer. The measured signal (in Volts) is then converted into a wavelength shift by dividing by the slope from Fig. S4-1a. This wavelength shift $\Delta\lambda$(nm) can then be converted into a MEMS beam displacement Δx(nm) using the relation $\Delta\lambda_j \approx 2\Delta x/(j+1)$, where the mode number j is related to the cavity length by $j=(2L_C n_C/\lambda)-1$. Our DBR mirrors have large refractive index contrast ($\Delta n_{Si\text{-}Air}$=3.5) and hence large reflectivity and bandwidth (BW>100 nm), so we can use this simple equation relating $\Delta\lambda$ and Δx.

In our device, L_C=100 µm and n_C=3.48 for silicon, which gives a mode number j=433. The absolute displacement for a drive signal RF=+5 dBm is shown in Fig. S4-1b and exhibits a peak displacement amplitude of 0.21 nm. The displacement is strongly dependent on actuation voltage (V^2). We emphasize that shorter cavities that exhibit higher finesse will have a stronger optical response for a given beam displacement, since shorter cavities exhibit a smaller mode number j while higher finesse implies a steeper slope. In fact, we have previously demonstrated MEMS Fabry-Perot devices with finesse F=265 (present devices: F=3.5) that enable measurement of the MEMS bridge thermal (Brownian) motion with *fm*/Hz$^{1/2}$ sensitivity and *picometer* absolute displacement [S-3].

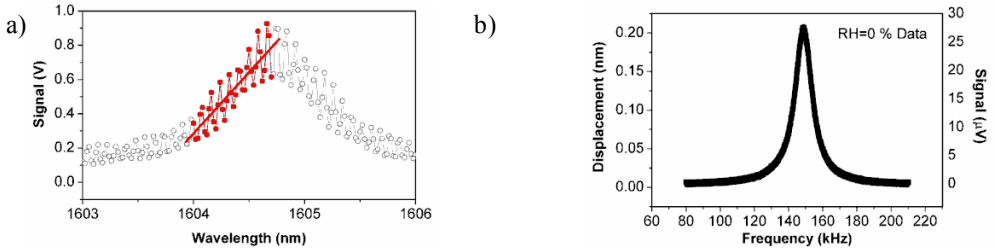

Fig. S4-1: a) Measured Fabry-Perot resonance and linear fit to extract maximum slope (laser power=1 mW), b) Extracted absolute beam displacement for a drive power RF=+5dBm (laser power=4 mW).

S.5 Static-Mode Sensing: Strain Loading

The present devices utilize a novel paddle design that helps to minimize the effects of polymer strain during absorption and mass-loading. On the other hand, for sensors operating in an aqueous environment (i.e. biological sensors) it may be advantageous to measure static displacements due to strain in the polymer. Figure S5-1a shows a simple fixed-fixed beam resonator with integrated Fabry-Perot cavity, similar to our MEMS-tunable Fabry-Perot filters [S-3]. The device does not have paddles and was coated with PEI across the entire beam top surface, with some polymer coating the beam sidewall. Upon exposure to water vapor, the Fabry-Perot optical resonances are shifted by $\Delta\lambda$=12 nm (Fig. S5-1b). We attribute the shift to an induced strain in the polymer as water vapor is adsorbed and the polymer swells [S-6]. The strain results in both *in-plane* and *vertical* beam bending; however, it is the *in-plane* bending that tunes the cavity. Using the relation $\Delta\lambda=2\Delta x/j$, where the mode number is $j=2L_C/(\lambda/n_{Silicon})$=16, we extract an *in-plane* beam bending Δx=96 nm due to polymer strain. Although the $\Delta\lambda$-tuning may be the result of refractive index tuning as water vapor enters the air gaps in the cavity, control experiments on uncoated fixed Fabry-Perot cavities indicate no significant resonant shifts ($\Delta\lambda\approx$0.01 nm, Fig. S5-2).

We also performed Fabry-Perot optical resonance measurements on the present sensors with paddles and long cavity, L_C=100 µm. The devices are coated with PEI, but only on the paddle regions. The measurements in Fig. S5-3 show no significant shift in the Fabry-Perot optical resonances in the presence of water vapor (RH=0-100 %). The invariance to induced strain results from two design changes: 1) the long cavity (L_C=100 µm) compared to the short cavity in Fig. S5-1 (L_C=3.5 µm) means that the new design is 28 times less sensitive to static beam displacements, and 2) the paddle's spring constant is large compared to the narrow MEMS beam so that any strain results in negligible beam bending, provided that the polymer is confined only to the paddles. The result in Fig. S5-3 confirms the effectiveness of our design for minimizing strain effects resulting from polymer swelling during absorption of chemical analytes. However, for sensors that operate in an aqueous environment static displacements due to strain may be useful (Fig. S5-1), provided the beam sidewall can be coated reliably.

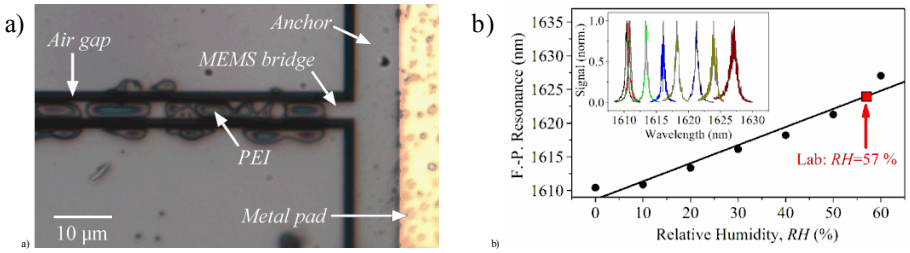

Fig. S5-1: a) Polymer (PEI) coating on a simple clamped-clamped beam resonator, similar to the devices in [S-3]. The polymer coats most of the beam surface and may also coat the beam sidewall, b) measured Fabry-Perot optical resonance shift vs. relative humidity (RH). The Fabry-Perot cavity length is L_C=3.5 µm and the MEMS beam has length L_{Beam}=400 µm and width W_{Beam}=3 µm [S-7].

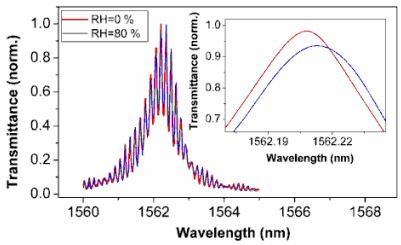

Fig. S5-2: Control experiment showing minimal Fabry-Perot optical resonance shift as a function of relative humidity (RH) for a fixed Fabry-Perot cavity with no polymer coating; the experiments rule out the role of refractive index tuning for the experiments in Fig. S5-1. The Fabry-Perot cavity length is L_C=3 µm.

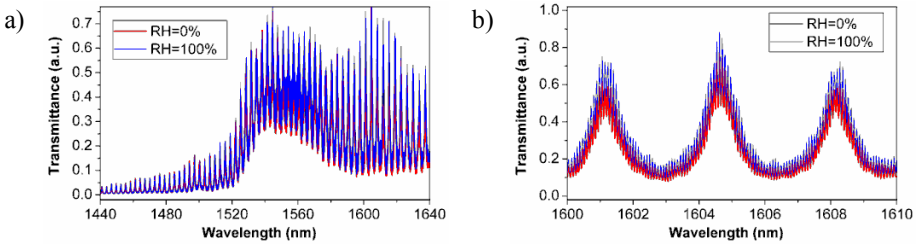

Fig. S5-3: Measured Fabry-Perot optical resonance vs. RH in the present device, where the polymer is coated only on dedicated paddles in order to minimize strain effects: a) full spectrum, b) detailed spectrum for 1600-1610 nm. The optical spectrum is unaffected by changes in RH, which indicates the effectiveness of the paddle design. The Fabry-Perot cavity length is L_C=100 µm and the MEMS beam has length L_{Beam}=300 µm and width W_{Beam}=1.5 µm.

S.6 Estimate of Polymer Coating Thickness

The deposited PEI thickness is estimated from optical white light profilometer measurements (Zygo Wyko Surface Profiler) on a test paddle with deposited PEI polymer. We measure an average polymer film thickness of 394 ± 23 nm on the paddle (Fig. S6-1). The PEI coating can vary considerably, however, with typical thicknesses ranging from around 100-800 nm, depending on surface area to be coated and polymer conditions. With improvements in preparation (i.e. polymer mixture and dilution), we expect better control over the thickness. Various other deposition techniques, including ink-jetting and dip pen lithography are also being explored [S-8].

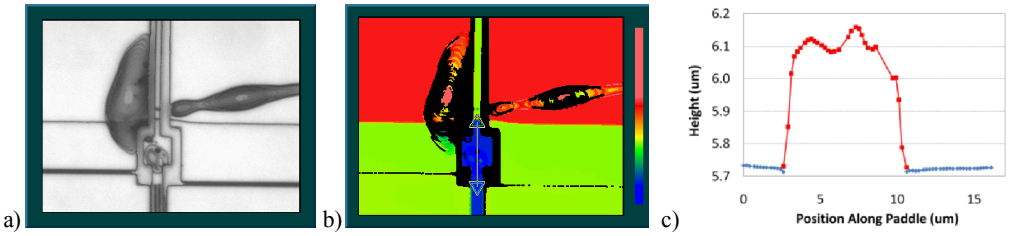

Fig. S6-1: Measured test paddle PEI polymer thickness using white light profilomtery: a) optical image, b) surface profile plot, c) line scan across PEI polymer on paddle region.

S.7 Transmission and Reflection Mode Sensing

The setup in Fig. 2 measures the transmitted signal from the Fabry-Perot cavity. However, the Fabry-Perot cavity also results in a reflected signal that is the complement to the transmitted signal, i.e. $R(L_C)=1-T(L_C)$, where $T(L_C)$ is given in eqn. (1). Consequently, we can also measure the reflected signal at the input side of the sensor in order to obtain the shift in mechanical resonant frequency as a function of mass loading. The experimental setup from Fig. 2 is modified by incorporating a fiber circulator at the input side to separate the input laser and reflected sensor signals. Measurements show that the transmitted (T_X) and reflected (R_X) signals are equivalent (Fig. S7-1). A significant difference, however, is that the transmitted signal will be determined by the resonant wavelengths of the Fabry-Perot cavity for each sensor; in contrast, the reflected signals will be determined by the reflection bandwidth of the input DBR mirror. This may result in a large cw signal on top of the modulated sensor signal at the reflected side. In contrast, the transmitted signal will be cleaner with only the modulated sensor signals present. Nonetheless, the ability to measure either the transmitted or reflected signal as demonstrated in Fig. S7-1 will facilitate the deployment of these types of sensors in existing fiber-optic networks.

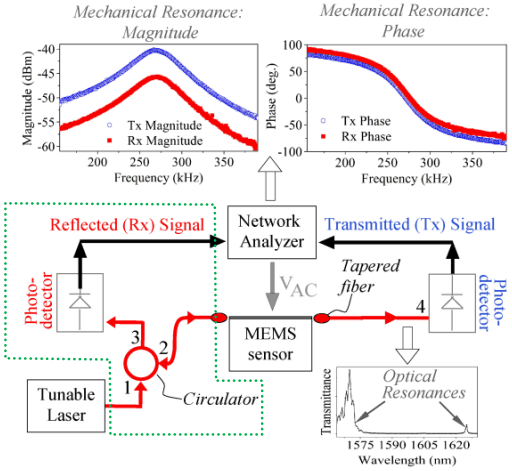

Fig. S7-1: Modified experimental setup enabling both the transmitted and reflected signal to be measured (dashed line). The input laser and reflected signals are separated using a fiber circulator (dashed line). Both transmitted and reflected signals give identical information, i.e. displacement amplitude and phase [S-7].

References:

[S-1] M. W. Pruessner, T. H. Stievater, W. S. Rabinovich, Preetpaul S. Devgan, and Vincent J. Urick, *Conf. Lasers & Electro-Optics (CLEO),* May 31-June 5, 2009, Baltimore, MD.
[S-2] M. W. Pruessner, T. H. Stievater, and W. S. Rabinovich, *Optics Lett.*, **32** (5) pp. 533-535, 2008.
[S-3] M. W. Pruessner, T. H. Stievater, and W. S. Rabinovich, *Appl. Phys. Lett.*, 2008, **92** (8), 081101.
[S-4] J.-M. Huang, K.M. Liew, C.H. Wong, S. Rajendran, M.J. Tan, A.Q. Liu, 2001, *Sens. Actuators A*, **93**, p.273-285.
[S-5] Siavash Pourkamali, Akinori Hashimura, Reza Abdolvand, Gavin K. Ho, Ahmet Erbil, and Farrokh Ayazi, *J. Microelectromech. Syst.*, Vol. 12 (4), pp. 487-496, 2003.
[S-6] A. Loui, T.V. Ratto, T.S. Wilson, S.K. McCall, E.V. Mukerjee, A.H. Love and B.R. Hart, *Analyst*, 2008, **133**, 608-615.
[S-7] M. W. Pruessner, T. H. Stievater, W. S. Rabinovich, J. L. Stepnowski, and R. A. McGill, *Proc. 15th Int. Conf. on Solid-State Sensors, Actuators and Microsystems (Transducers)*, June 21-25, 2009, Denver, CO.
[S-8] A. Higgins, E. J. Houser, M. R. Papantonakis, V. Nguyen, S. V. Stepnowski, T. H. Stievater, W. S. Rabinovich, N. A. Papanicolau, R. Bass, J. L. Stepnowski, M. T. Rake, "Sorbent Coatings and Processing Techniques for Trace Analysis of Hazardous Materials in Micro/Nano Sensors," *17th University/Government/Industry Micro/Nano Symposium*, 2008.